UNIVERSITY OF TARTU

Faculty of Science and Technology

Institute of Technology

Thi Bich Phuong Nguyen

Modelling of a Yeast-contained Material

Bachelor's Thesis (12 ECTS)

Curriculum Science and Technology

Supervisor:
Ph.D., Vahur Zadin

Tartu 2020

Abstract

Modelling of a Yeast-contained Material
Thi Bich Phuong Nguyen
University of Tartu, Institute of Technology
Bachelor's thesis 2020, 43 p. + 6 p. appendixes
Supervisor: Ph.D. Vahur Zadin

This work introduces a computational model to study the properties of a novel yeast-contained material. The model considers the catalysis properties of the material in converting glucose to fermentation products, mass transportation in the material, and the material's mechanical properties. The model provides insights regarding the characteristics and behaviors of the material, putting a stepping-stone for further development in experiments. The study uses three different simulation methods, in particular a simple numerical model, a 2D and a 3D finite element model. The overview of the material, theoretical background, and the simulation methods accompanying the models are discussed in this thesis. The model forms a quantitative prototype to study the catalysis property of the material in glucose fermentation.

Keywords: yeasts, glucose fermentation, living material, numerical simulation, finite element method, mass transportation, solid mechanics.

CERCS: T150

Lühikokkuvõte

Pärmipõhiste elusmaterjalide arvutisimulatsioonid

Käesolev bakalaureusetöö keskendub uudse, pärmi sisaldava elusmaterjali, uurimisele arvutisimulatsioonide abil. Töö tulemusena on loodud prototüüpmudel mis võimaldab uurida materjali katalüütilisi omadusi glükoosi fermenteerimisprotsessi käigus. Mudel võtab arvesse materjali massitranspordi piiranguid ja mehaanilisi omadusi ning selles tulenevaid reaktsioone piiravaid faktoreid võimaldades jälgida glükoosi konverteerimisprotsessis fermentatsiooniproduktideks. Mudel võimaldab uurida materjali omadusi ja selle käitumist ning on hüppelaud edasisteks eksperimentaalseteks arendusteks. Uuringus kasutatakse kolme erinevat simulatsioonimeetodid: lihtsustatud numbrilist mudelit, seejärel kahe- ja kolmemõõtmelisi lõplike elementide meetodil baseeruvaid mudeleid. Käesolev väitekiri annab detailse ülevaate uuritud materjalist, kasutatud ja arendatud mudelite teoreetilisest taustast ja rakendatud simulatsioonimeetodtest.

Märksõnad: Pärm, glükoosi fermenteerimine, elusmaterjal, arvutisimulatsioon, lõplike elementide meetod, massitransport, tahkise mehaanika.

CERCS: T150

Contents

Notations

Notation	Unit	Explanation
A_G	$1/s$	The frequency factor of the fermentation reaction
E_a	J/mol	The activation energy of the fermentation reaction
T	$^\circ C$	Temperature
A_{IG}	mol/m^3	The frequency factor of glucose inhibition
E_I	J/mol	The activation energy of glucose inhibition
K_x	mol^2/m^6	The yeast growth inhibition constant
K_{GL}	h^{-1}	The gas to liquid transfer coefficient
$c_{CO2(sat)}$	mol/m^3	The saturated carbon dioxide concentration in water
Y_x		The yield coefficient of yeast
Y_E		The yield coefficient of ethanol
Y_{CO2}		The yield coefficient of carbon dioxide
Y_{Ac}		The yield coefficient of acetic acid
Y_G		The consuming coefficient of glucose
μ	h^{-1}	The specific growth rate of yeast
$\mu_{X_{max}}$	h^{-1}	The maximum specific growth rate of yeast
K_G	g/L	The half-velocity constant
$I_{G/X}$	g/L	The glucose inhibition constant for yeast growing
$c_{E_{max}/X}$	g/L	The maximum ethanol concentration for yeast growing
$\mu_{E_{max}}$	h^{-1}	The maximum specific producing rate of ethanol
K_E	g/L	The ethanol saturation constant
$I_{G/E}$	g/L	The glucose inhibition constant for ethanol production
$c_{E_{max}/E}$	g/L	The maximum ethanol concentration for ethanol production
$Y_{X/G}$	g/g	The yeast yield coefficient
$Y_{E/G}$	g/g	The ethanol yield coefficient
m	h^{-1}	The cell maintenance coefficient
α	g/L	The ethanol inhibition constant
β	g/L	The ethanol inhibition constant

Chapter 1

Introduction

Yeasts are organisms involved in many science and engineering processes, especially in the fermentation applications, due to the ability of fermenting a wide range of sugars. By infusing a hydrogel with living yeasts and then using the gel as a material for three-dimensional printing, scientists produced a yeast-contained material that can ferment sugar into ethanol continuously, vigorously (Saha et al., 2018; Priks et al., 2020). This novel material has promising applicability for wearable devices, biosensors, drug-releasing surfaces, and biocatalysis applications (Liu et al., 2017).

While the production of such material is obtainable, the properties of the material and its behaviors during the fermentation process are unclear yet. Developing a computational model to understand the material properties, especially its catalytic activity in the sugar fermentation processes, is crucial to facilitate the synthesis of application-specific polymers and the design of advanced living materials in the future .

The aims of the thesis

The aim of this study is to develop a model that studies essential chemical and physical properties of the yeast-contained material when the material involves in the glucose fermentation. The model reflects three important material properties.
The first one is the catalysis property of the material in converting glucose to fermented products through fermentation. During this process, the yeast biomass also increases via cell divisions. Secondly, geometry and mass transportation in the material and its effects on the fermentation process were considered. The mass transportation in the material, governed mainly by diffusion and convection, is an important factor that affects the fermentation reaction rates of yeast in different locations. The transport includes the internal moving of molecules inside the material and the exchange of molecules between material surrounding aqueous environment. Thirdly, the model took into account the mechanical properties of the material and its effects on the fermentation

process. When the number of yeast cells increased, the volume of yeasts was expanded, causing stress to the material, especially the areas surrounding the yeast domains. Since the yeast has its own critical stress, when the stress reached this critical value, the yeast stopped its divisions (SP et al., 2018). In fact, the mechanical process is one important part of the model which determines the sustainability of target materials. Figure 1.1 gives an overview of essential processes in the model.

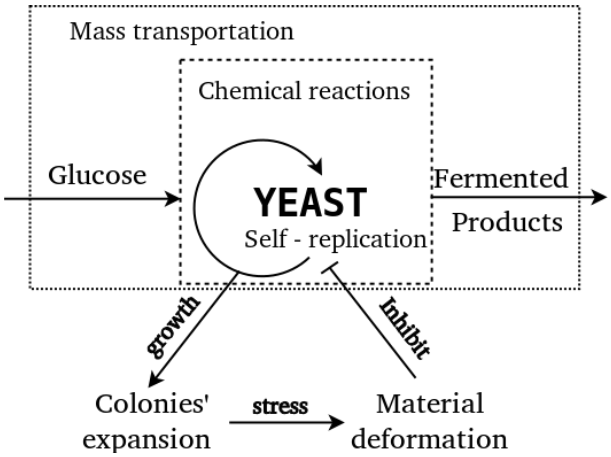

Figure 1.1: Processes in the model

My contributions

My main contributions in this study are introducing and optimizing a fermentation-processing model of the material based on previous kinetics studies (Ramirez, 1994; Ramirez and Maciejowski, 2012; Ariyajaroenwong et al., 2016; Andrews, 1968; Zentou et al., 2019). In addition, other inhibit factors to the fermentation process, such as mass transportation and mechanical properties of the material, were taken into account. The model was deployed conscientiously with a numerical model and finite element models.

Work flow

Developing the model following these steps: Firstly, a numerical model was deployed which mainly focused on the fermentation reactions with free-mobilized yeast. Secondly, in addition to the fermentation process, the immobilized yeast and other limited transportation factors were introduced to the finite element model 1. Finally, the material's mechanic properties were taken into consideration with other factors, presented in the finite element model 2.

Chapter 2

Overview of the material

2.1 S. Cerevisiae Yeast

Yeasts are single-cell microorganisms which belong to the kingdom of fungi. There are more than 1500 species of yeasts have been discovered over thousands of years of humankind (Piskur and Compagno, 2004). Typically, the size of yeasts varies from 3-4 μm in diameter, depends on the type of yeast and its living environment. Most yeasts reproduce asexually by mitosis through an asymmetric division process known as budding. Yeasts are chemoorganoheterotroph species which require only organics compound as their main energy or carbon source. Their common carbon sources are hexoses (glucose and fructose) or disaccharides (sucrose, maltose). To extract energy from those compound, reduction-oxidation reactions are involved which can either go through an aerobic process with oxygen present or an anaerobic where no oxygen is allowed.

The most popular yeast species are the Saccharomyces cerevisiae which can converts sugars to ethanol and carbon dioxide through a process called fermentation. Traditionally, S. cerevisiae has been used widely in the production of alcoholic beverages such as beers or wines. It is also used in baking as a leavening agent which helps the baked products remain soft and spongy.

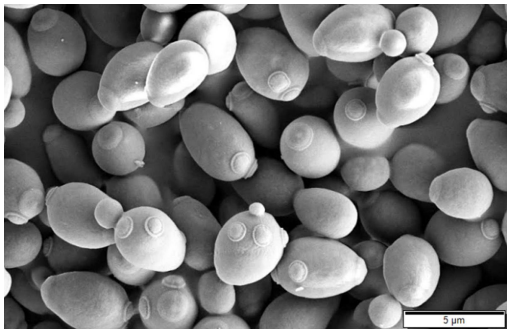

Figure 2.1: A micrograph of the S. cerevisiae (Murtey and Ramasamy, 2016).

Nowadays, S. Cerevisiae becomes an essential organism, an important component not only

in engineering fields but also in scientific researches. In chemical environmental engineering, S. Cerevisiae acts as a bio-remediator for removal of metal from polluted water waste (Malik, 2004) or reduction of phenolics, chemical oxygen demand, and antimicrobial compounds in olive old mill wastewater (Bleve et al., 2011). In chemistry, S. Cerevisiae catalyzes for the synthesis of compounds for fine chemical and active pharmaceutical ingredients (B and A., 2008). In biotechnology, S.Cerevisiae is utilized in protein production and genetic analysis (GP and JM., 1999).

2.2 Yeast-contained material

Introducing a material that contains immobilized yeast cells is a vital path to enhance the production of target synthesized compounds as well as the purity of the final products (Li et al., 2008; PM and JE., 1986). In addition, this novel material has a higher capability to apply to different high-end applications such as tissue engineering scaffolds (Zhu and Marchant, 2011), controlled drug delivery (Li and Mooney, 2016), due to higher robustness and reproducibility (Saha et al., 2018).

A group of researchers from the Institute of Technology, University of Tartu re-produced successfully yeast-contained materials in which hydrogels were used as an encapsulator to constrain living S. Cerevisiae yeasts (Priks et al., 2020). Figure 2.2 shows photographs of this material which has a perimeter form with dimensions about 10x3x5 mm. Figure 2.3 presents the micrographs of the yeast-contained material in which the yeast cells are homogeneously distributed in the hydrogel matrix.

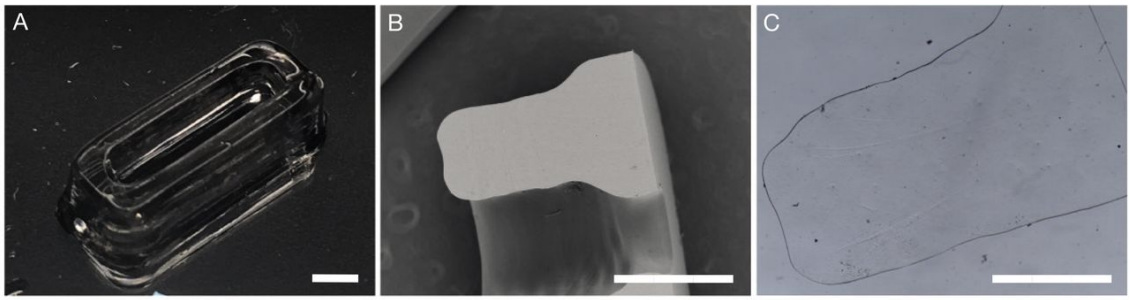

Figure 2.2: The structure of the material (without yeast cells); A: a photograph of the stabilized material, B: Cross-sectional micrograph, C: slice micrograph. Scale bar 1mm (Priks et al., 2020).

To have a better understanding of the material, a procedure to produce a cubic of yeast-contained material had done by the (Saha et al., 2018) is illustrated in Figure 2.4. In this procedure, 2.5g F127-dimethacrylate (F127-DMA) was dissolved in the 7.5g SC media and cooled at 4°C overnight to prepare 25 wt % F127-DMA hydrogels. The hydrogel mixture underwent a transition from gel to sol, forming a viscous liquid. The next step, yeast cells were extracted from 10ml of yeast-contained SC media, each of them has around 10^6 cells, and added to the hydrogel solution. In

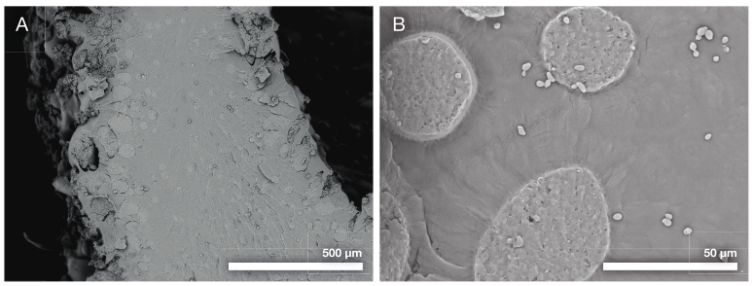

Figure 2.3: Micrograph of the yeast-contained material (Priks et al., 2020).

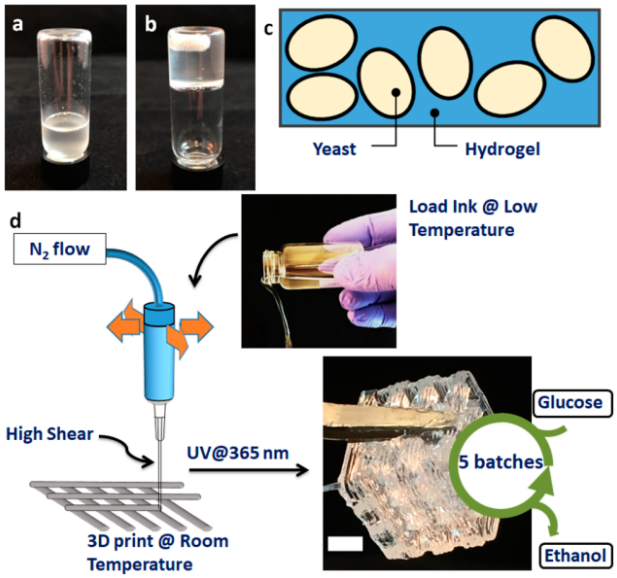

Figure 2.4: Overview of the process: The F127-DMA hydrogels (25 wt %) in SC media occupied a "sol" state at (a) 4°C and a "gel" state at (b) 23°C. Graphical representation of the (c) yeast-laden hydrogel ink for the (d) direct-write 3D printing of cube lattice capable of biocatalytic conversion of glucose into ethanol for five batches (Scale bar: 5 mm) (Saha et al., 2018).

addition, the photo radical generator was added. The mixture was mixed carefully to create a homogeneous solution, which was warmed up to the room temperature producing a shear-responsive gel, ready for the printing process. For the printing process, the direct-wire 3D printing was performed with the dimensions of printed-cubic are 15mm and its weight is about 2.64g. The printed cube was exploded to a radiation source (365 nm in wavelength) to cure and chemically fix the structures, then it went through another post-treatment to obtain the multilayered structure.

2.3 Catalysis property of the material

The printed yeast-contained material showed a stable activity in catalysis of the fermentation process which converts glucose to ethanol in a batch over two weeks (Saha et al., 2018; Priks et al.,

2020) also investigated the catalysibility of the material in fermentation through the experiments as below.

A perimeter of a printed the yeast-contained hydrogel was transferred to a flask which contained 40mL of glucose solution. The initial glucose concentration is 10.347 g/L and the initial number of yeast cells in the cubic is 10^5, with or without an air supply. The fermentation was carried out at 25°C under static conditions to prevent the detachment of the yeast cells from the hydrogel matrix. Samples were taken for analysis at regular time intervals. Table A.1 provides information about the concentrations of remained glucose, fermentation products, and biomass after 48h of cultivation. There is no significant difference in the products' concentration between the experiments with air supply and the one without air supply.

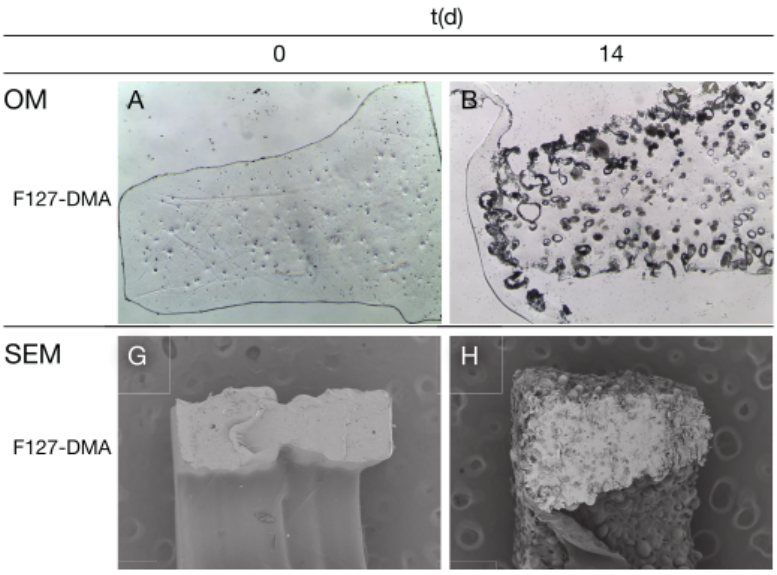

Figure 2.5: Micrographs of the material before and after cultivation time (Priks et al., 2020).

Figure 2.5 presented micrographs of the material before and after the cultivation time in which the number of yeast cells increased tremendously and occupied more volume portion of the material. The appearance and volume of the perimeter were also changed when comparing between Figure 2.5G and 2.5H.

Chapter 3

Methods

3.1 Chemical and physical background

3.1.1 Fermentation models

a. Numerical model

A numerical model was studied in which only focuses on the fermentation process in a batch mode with the following assumptions:

- The yeast cells are uniformly distributed in the medium with no traveling restrictions. In other words, the initial yeast cells are considered to spread the whole medium without the present of the hydrogel matrix.
- The mixture of yeast cells, glucose, and fermented products are mixed properly so that the fermentation reaction is not limited by molecular transportation factors.
- The temperature of the whole mixture is constant.

The model can be validated by comparing the model's output with the experimental number of yeast cells, concentration of reactant, and products at the Table A.1.

To obtain the best suitable fermentation model for the material, existed models from previous studies were referred (Ramirez, 1994; Ramirez and Maciejowski, 2012; Ariyajaroenwong et al., 2016; Andrews, 1968; Zentou et al., 2019). This work re-produced two fermentation models with adjustments.

The Fermentation model 1 was referred from the Beer brewing model (Ramirez, 1994; Ramirez and Maciejowski, 2012; COMSOL, Inc., 2015) simulating the glucose fermentation process which converts glucose to ethanol, acetic acid, and carbon dioxide, taking into account only glucose inhibition. Since the model presented a fermentation process in a tank of beer in the industrial

procedure, the volume and concentration scales are largely leading to a large tolerance. The model is less applicable in the case of a small system.

The Fermentation model 2 is referred from the previous researches (Ariyajaroenwong et al., 2016; Zentou et al., 2019) which introduced a fermentation model of immobilized-yeast. In this model, the yeast immobility factor, glucose limitation, glucose inhibition, ethanol inhibition, and cell death are taken into consideration.This model is different from the fermentation model 1 at three main points. Firstly, the immobility of yeasts was introduced in the model, which effects profoundly on the reactions rate. Secondly, it considered the glucose and ethanol inhibitions as important factors effecting to the fermentation process. In fact, if the initial concentration of glucose or ethanol are too high, it inhibits yeast growing in a non-competitive manner (Aiba et al., 1968). Besides, the model was simulated in a small-scale volume which works more accurately corresponding to our experiment setup.

The two fermentation models were first reproduced from the original works with the same initial conditions for validations. After that, the models were setup and optimized with the experiment data from section 2.3.

b. Fermentation model 1

The reactions in this system mimic to the fermentation reactions in the brewing beer process. Thus, this fermentation model was referred from the Beer brewing model (Ramirez, 1994; Ramirez and Maciejowski, 2012; COMSOL, Inc., 2015).

The fermentation reaction is described as:

$$G \xrightarrow{X} E + Ac + CO_2$$

G, X, E, Ac denotes for Glucose, Yeast, Ethanol, and Acetic acid. The reaction kinetics are considered as:

$$r = k.c_x \tag{3.1}$$

The fermentation mechanisms depend on the yeast concentration and the reaction rate k. The Michaelis-Menten kinetics or enzyme kinetics defined the rate of reactions k (Mathews et al., 1999), mathematically as:

$$k = \frac{k_G.c_G}{K_G + c_G} \tag{3.2}$$

k_G is the maximum initial reaction rate, K_G is the Michaelis-Menten constant which is equal to the substrate concentration at which the reaction rate is half of the k_G value (Mathews et al., 1999). According to the Arhenius equation which describes the dependence of reaction rate constant to the temperature in which the reaction takes place (Laidler, 1987), the k_G and K_G are determined as:

$$k_G = A_G.e^{\frac{-Ea}{RT}} \tag{3.3}$$

$$K_G = A_{IG}.e^{\frac{-E_I}{RT}} \tag{3.4}$$

where A_G, A_{IG} are frequency factors; E_a and E_I are activation energy and inhibition energy of the fermentation process, respectively. The temperature was assumed unchanged thus those constants would not change responding to the temperature during the fermentation process.

The yeast concentration was studied a free-species (COMSOL, Inc., 2015), its reaction-rate is described:

$$R_x = k_x.c_x \tag{3.5}$$

where k_x is reaction rate constant that depends on the reaction of glucose and the fact that the yeast concentration inhibits its production:

$$k_x = Y_x.k.\frac{K_x}{K_x + (c_x - c_{x0})^2} \tag{3.6}$$

Y_x is the yield coefficients, K_X is the yeast growth inhibition constant, c_{x0} is the initial yeast concentration.

From Eq. 3.5, 3.6, the reaction rate of yeast could be summarized as:

$$R_x = Y_x.k.\frac{K_x}{K_x + (c_x - c_{x0})^2}.c_x \tag{3.7}$$

The alcohol production is related to the yield coefficient, leading to the following production rate:

$$R_E = Y_E.k.c_x \tag{3.8}$$

With the same philosophy, the production rate of acetic acid is calculated as:

$$R_{Ac} = Y_{Ac}.k.c_x \tag{3.9}$$

For carbon dioxide, both gaseous and dissolved species are taken into account. The production rate of the gaseous one is described by:

$$R_{CO2(g)} = Y_{CO2}.k.c_x - K_{GL}.(c_{CO2(sat)} - c_{CO2(l)}) \tag{3.10}$$

Where K_{KL} is the gas to liquid mass transfer coefficient of carbon dioxide and $c_{CO2(sat)}$ is the concentration of carbon dioxide in saturated solution with water.

For the dissolved species, the reaction rate is:

$$R_{CO2(l)} = -K_{KL}.(c_{CO2(sat)} - c_{CO2(l)}) \tag{3.11}$$

Finally, the consuming rate of Glucose depends on the reaction rate and a consuming coefficient as:

$$R_G = -Y_G.k.c_x \tag{3.12}$$

The model was developed with the parameters given in Table A.2.

c. Fermentation model 2

The fermentation reaction is described as:

$$G \xrightarrow{X} E + CO_2$$

The Monod empirical equation describes the relation between growth rates of microorganisms and concentration and nutrient source, written as:

$$\mu_X = \frac{\mu_{X_{max}}.c_G}{K_G + c_G} \tag{3.13}$$

Where μ_X and $\mu_{X_{max}}$ is the specific growth rate and the maximum specific growth rate of the microorganisms - yeast. c_G is the concentration of the nutrient source - glucose in this case. K_G is the half-velocity constant and can be specified by the value of c_G when $R_X/R_{X_{max}} = 0.5$. Thus, both $R_{X_{max}}$ and K_G are empirical coefficients from experiments and depends on either the living species or growth environmental conditions.

The equation 3.13 does not consider the inhibitory factors of substrate and product to the growth of the living yeast, which is critical in our model case. To add those factors to the model, (Andrews, 1968; Levenspiel, 1980) proposed:

$$\mu_X = \left(\frac{\mu_{X_{max}}.c_G}{K_G + c_G + \frac{\chi^2}{I_{G/X}}}\right)\left(1 - \frac{c_E}{c_{E_{max}/X}}\right)^{\alpha} \tag{3.14}$$

$I_{G/X}$ is the glucose inhibition constant for yeast growing, χ^2 is the reduced chi-squared, c_E is the current ethanol concentration, $c_{E_{max}/X}$ is the maximum ethanol concentration in which living yeast are still able to grow, and α is the ethanol inhibition constant.

In addition, a pressure limiting factor is added to the yeast growth rate to investigate how this factor affects to the fermentation, formulated as:

$$\mu_X = \left(\frac{\mu_{X_{max}}.c_G}{K_G + c_G + \frac{\chi^2}{I_{G/X}}}\right)\left(1 - \frac{c_E}{c_{E_{max}/X}}\right)^{\alpha}\left(1 - \frac{P}{P_{max}}\right) \tag{3.15}$$

Where P is the current pressure on yeast, P_{max} is the critical pressure at which yeasts stop to grow.

In this fermentation process, ethanol is the primary product and its production is associated with yeast growth-rate. Under Andrew's philosophy, the ethanol production rate can be calculated as:

$$\mu_E = \left(\frac{\mu_{E_{max}}.c_G}{K_E + c_G + \frac{\chi^2}{I_{G/E}}}\right)\left(1 - \frac{c_E}{c_{E_{max}/E}}\right)^{\beta} \tag{3.16}$$

K_E is ethanol saturation constant, $I_{G/E}$ is the glucose inhibition constant for ethanol formation, $c_{E_{max}/E}$ is the maximum ethanol concentration in which ethanol fermentation still occurs, and β is the ethanol inhibition constant.

Following the kinetics of chemical reactions, the yeast growth rate and ethanol production rate can be computed as follow:

$$R_X = \frac{dX}{dt} = \mu_X . c_X \tag{3.17}$$

$$R_E = \frac{dE}{dt} = \mu_E . c_X \tag{3.18}$$

From Eq. 3.15, 3.16, 3.17, 3.18, the reaction rates of yeast and ethanol can be summarized as:

$$R_X = \left(\frac{\mu_{X_{max}} . c_G}{K_G + c_G + \frac{\chi^2}{I_{G/X}}} \right) \left(1 - \frac{c_E}{c_{E_{max}/X}} \right)^{\alpha} \left(1 - \frac{P}{P_{max}} \right) c_X \tag{3.19}$$

$$R_E = \left(\frac{\mu_{E_{max}} . c_G}{K_E + c_G + \frac{\chi^2}{I_{G/E}}} \right) \left(1 - \frac{c_E}{c_{E_{max}/E}} \right)^{\beta} c_X \tag{3.20}$$

During the fermentation, glucose is consumed in the process of yeast growing and living and ethanol production. Thus, glucose consumption can be calculated as:

$$R_G = -\frac{dG}{dt} = \frac{1}{Y_{X/G}} R_X + mX + \frac{1}{Y_{E/G}} R_E \tag{3.21}$$

$Y_{X/G}$ and $Y_{E/G}$ is the yeast and ethanol yield coefficient, respectively; m is the yeast maintenance coefficient.

The constant and coefficient in the above equations were determined experimentally in Ariyajaroenwong et al. (2016) and presented at Table A.2.

3.1.2 Mass transport equations

a. Fick's laws - Diffusion equations

Diffusion is the motion of one or more particles of a system relative to other particles. It occurs in all materials at all times at temperatures above absolute zero (Onsager, 1945). In a solution, solute molecules could move continuously from one area to another area forming a homogeneous system. This process can be driven by the concentration gradient, temperature gradient, or electric field. In 1855, Adolf Fick proposed 2 laws to describe this phenomenon. 2 those laws later were derived and well-known as diffusion equations (Fick, 1995).

The Fick's first law characterizes the diffusion occurring in response to a concentration gradient. In other words, it can be concerned as the change in the concentration corresponding to the change in positions. The diffusive flux (J) goes from regions with higher concentration to regions with lower concentration is proportional to the concentration gradient, can be written as:

$$J = -D\frac{d\omega}{dx} \tag{3.22}$$

D is the diffusion coefficient and usually expressed in a unit of m^2/s. D is determined from experiments and depends on the material and physical conditions. ω is a substance concentration - amount of substance per unit volume. The common unit of concentration is mol/m^3. x is the position in the length (1D) dimensions and have m unit. The diffusion flux (J) has the unit of $mol/(m^2.s)$ that expressed the amount of substance crosses a unit area in a certain time. In the case of diffusion of the system having more than one dimension, the gradient operator ∇ is used which implies the first derivatives of concentration to all dimensions.

$$J = -D\nabla\omega \qquad \text{or} \qquad J = -D\omega'(x,y,z) \tag{3.23}$$

The Fick's first law describes the relation of substance's concentration and the concerned position. However, the law is only applicable to the system in a steady state. When the concentration not only depends on the studied position but also the time, the second law of diffusion should be used.

The second law is about how the diffusion process drives the change in concentration by time. In one dimension, the law is expressed as:

$$\frac{\partial\omega}{\partial t} = D\frac{\partial^2\omega}{\partial x^2} \tag{3.24}$$

ω is concentration described as a function of time and position - $\omega(x,t)$ - with the unit of mol/m^3. t is time in second and x is the position coordinators in meter. The law could be written as the concentration's accumulation is proportional to the curvature of the concentration gradient. The higher the curvature of the gradient, the higher the accumulation rate of concentration.

b. Convection - diffusion equation

In a liquid, the movement of bulk of fluid could drive the mass transfer processes. This mechanism of transportation is named as convection. One example is the ocean currents. Those ocean currents - directed movements of seawater - carry a massive amount of biomass and aquariums to different destinations in the world.

The convection is concerned as the movement resulting from the average velocity of all molecules in the fluid. This is the main different between convection and diffusion where transportation depends on the Brownian motion (Chapter 3.1.2.b).

The power of convection and its direction is indicated by the convective flux. In the case of a diluted solution, the velocity of dominant component (solvent) is chosen as a reference velocity to identify the convection flux of a diluted species (N), contributing as:

$$N_{i,conv} = c_i u \tag{3.25}$$

where u is the solution's velocity (m/s), c_i is the concentration of a species ($mol.m^{-3}$). The convective flux is therefore proportional to the velocity of the solution of the solvent.

In a solution, it is common that a species is transported by both mechanisms - diffusion and convection. Combining 2 equations could make the simulation process simpler.

In the medium, the mass flux N of the i species is sum of diffusive flux J and convective flux $N_{i,conv}$, formulated as:

$$N_i = J + N_{i.conv} \tag{3.26}$$

From 3.23 and 3.25:

$$N_i = -D\nabla\omega - c_i u \tag{3.27}$$

The equation is the boundary condition for the mass balance equation we would discuss later.

c. Mass conservation

In an isolated system - a thermodynamic system that neither mass nor energy can be exchanged - the measurable properties would be constant all the time. This is the content of the conservation law which can be applied to energy, different momentums, and approximately applied to the mass. In fluid dynamics, one common form of the conservation law is given by a continuity equation, written in a differential form:

$$\frac{\partial c_i}{\partial t} + \nabla \cdot N_i = R_i \tag{3.28}$$

Where c_i is the concentration of i, $\nabla\cdot$ is divergence, N_i is total flux (sum of diffusive and convective fluxes), R_i is the production rate of that species in the chemical reactions.

From 3.27 follows:

$$\nabla \cdot N_i = \nabla \cdot (-D\nabla\omega) - \nabla \cdot (c_i u) \tag{3.29}$$

And:

$$\nabla \cdot (c_i u) = \nabla \cdot c_i u + c_i \nabla \cdot u$$

In this model, the solution does not change its density during the flow. This flow can be considered as incompressible fluid flow. Thus, the velocity divergence $\nabla \cdot u$ is equal to zero. The 3.29 can be re-written as:

$$\nabla \cdot N_i = \nabla \cdot (-D\nabla\omega) - \nabla \cdot c_i u \tag{3.30}$$

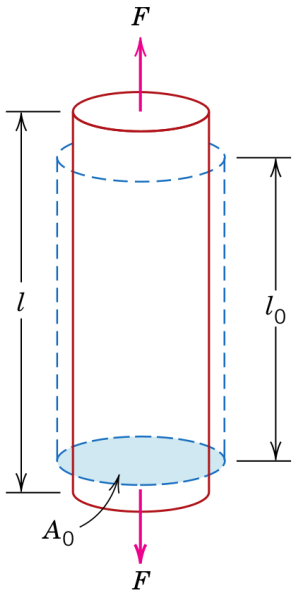

Figure 3.1: Schematic illustration of how a tensile load produces elongation and positive linear strain. Dashed lines represent the shape before deformation; solid lines, after deformation (William D. Callister, 2007).

Replacing $\nabla \cdot N_i$ in 3.28, we get:

$$\frac{\partial c_i}{\partial t} + \nabla \cdot (-D\nabla\omega) - \nabla \cdot c_i u = R_i \tag{3.31}$$

The $\partial c_i/\partial t$ presents for the change in the concentration of solutes. The $\nabla \cdot (-D\Delta c_i)$ describes the diffusion that depends on the diffusion coefficient and concentration (follows Fick's Law). The third element, $\nabla \cdot c_i u$, correspond to the convective transport, where u is the velocity field. On the right hand, R_i is source of solute that is resulted from chemical reactions.

In this model, equation 3.31 determines the change in concentration of any species at a given time and given location due to the reduction/consumption of chemical reactions and mass transportations0.

3.1.3 Solid mechanics

a. Elastic properties of materials

Materials, in general, are usually subjected to forces or loads. Determining the mechanical properties of a material is an essential step that helps to choose the right materials for any objects to avoid fractions or disruptions. The tensile test is a common way to determine mechanical stress and strain, from which many other properties can be ascertained, especially elasticity. Figure 3.1 gives an overview of the tensile test in which a load is changed relatively slow and applied to a uniform cross-section of a testing object, called specimen. The test is often conducting in the way

that the specimen is elongated at a constant rate while the applied loads and resulting elongations are continuously, simultaneously measured.

Since the load-elongation relation depends on the size of the specimen i.e. the cross-section area, the engineering stress, and engineering strain are used to normalize the geometry factors. The mechanical stress is defined as:

$$\sigma = \frac{F}{A_0} \tag{3.32}$$

in which F is the force applied perpendicularly to the specimen cross-section, in units of newtons (N), and A_0 is the area of cross-section with the units of squared meters (m^2). The units of mechanical stress are newtons per squared meters (N/m^2) or Pascal (Pa).

The engineering strain is determined according to:

$$\varepsilon = \frac{l - l_0}{l_0} = \frac{\Delta l}{l_0} \tag{3.33}$$

in which l is the elongated length while l_0 is the original length of the specimens. The strain is unitless and its value does not depend on the unit system.

The strain determines the degree of deformation of materials according to an imposed stress. The relation between engineering stress and engineering strain for elastic deformation is described by Hooke's law as follow:

$$\sigma = E\varepsilon \tag{3.34}$$

The constant of proportionality E is called modulus of elasticity or Young's modulus which has the units of pascal (Pa). The young's modulus emphasizes the ability of a material to withstand changes in length when under lengthwise tension or compression. For metal, Young's modulus is ranging from 50 GPa to 400GPa. For the hydrogel with hydrogen bond reconstruction post-treatments, the value is 0.59-1.94 MPa (Zhu et al., 2017) .

b. Volume expansion

The growth of yeast cells and its replication processes lead to the expansion of yeast colonies' volume, result in stress on the hydrogel background. This phenomenon is mainly caused by the yeast replication process. To model this process, the train of the polymer around the yeast colonies areas is studied, and mathematically described as:

$$\varepsilon = \beta_v . \Delta n_{cells} \tag{3.35}$$

Where β_v is the coefficient of the volume expansion and Δn_{cells} is the difference between the number of yeast cells at the beginning comparing to the one at the time of the study.

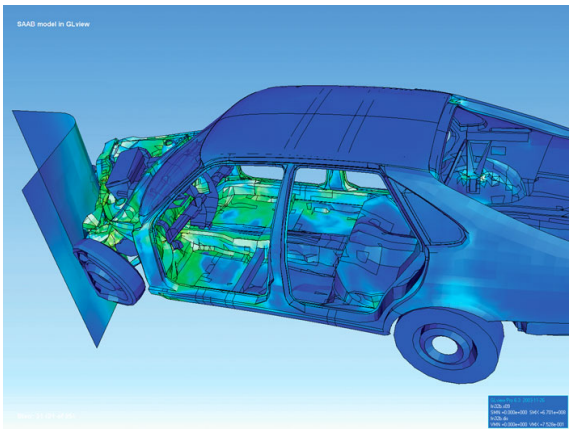

(a) Deformation of a car in a cash using finite element analysis (Logan, 2011).

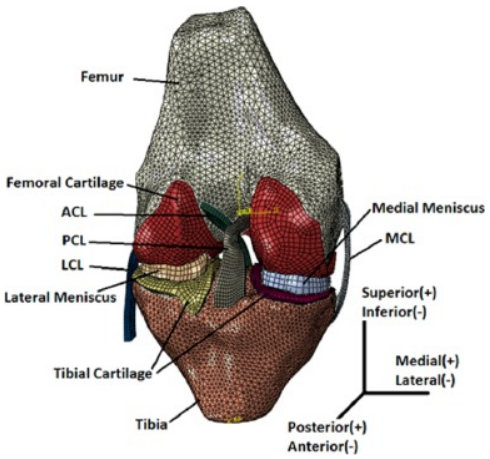

(b) Finite element model of a human knee joint (Beidokhti] et al., 2016).

Figure 3.2: Finite element simulations in science and engineering.

3.2 Finite element method

In simulation science, some objects are either too large or too complicated to simulate all components in one model. Thus, a numerical method was developed to analyze those problems where the target objects are subdivided to the smaller components called "elements". By understanding the elements' behaviors, the original simulating objects could be rebuilt with highly understandable properties for the whole phenomenon (Entwistle, 2001). The process above describes the Finite element method (FEM). With this simulation method, many natural processes can be sufficiently well described on the macroscopic level, without taking into account the individual behavior of molecules, atoms, electrons, or other particles.

Nowadays, FEM is widely used in science and engineering. For instance, in science, human knee joints were studied with finite element analysis (Beidokhti] et al., 2016); in the vehicle industry, this analysis method was used in the simulation of a car's deformation in cash in preparation for car productions (Logan, 2011) (Figure 3.2).

3.2.1 Partial differential equation

The target properties of the studied system have to be able to be approximated as Partial differential equations (PDEs). There are many such equations in engineering fields, for example, the mass transport equation, the equation of fluid flow, and the equation of electromagnetic potential, etc. For a simplified physical model, a simple PDE is assigned for each element with its boundary conditions. The assembly of the whole system results in a system of algebraic equations that can be calculated by a computer. By using many approximations and simplification method the matrix of studied properties could be solved giving approximate solutions of boundary value problems

(Solin, 2016).

3.2.2 Mesh

The body system is firstly divided into discrete connected parts called Finite elements. This process terms Discretisation. The pattern of elements is called Mesh. For the 2D models, the elements are commonly triangles or quadrilaterals. For the 3D models, the elements could be tetrahedral or parallelepiped. Choosing the mesh and elements' size depends on the experiences, problems, resources, and requirements for the calculation. The finer mesh, the more accuracy, the heavier calculations.

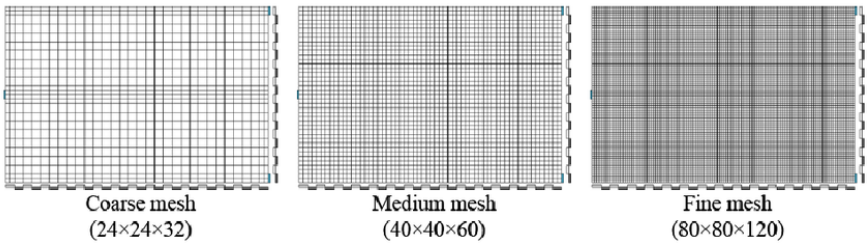

Figure 3.3: Three different types of mesh design (Ito et al., 2015).

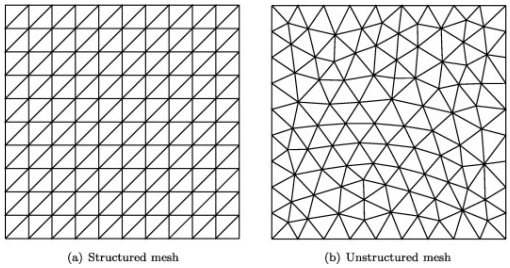

Figure 3.4: Dfferent types of the triangular mesh (Hiester et al., 2014).

3.2.3 Finite element

An adequate model could be obtained using a finite number of well-defined elements where these elements are contributors with a certain weight. Consider a linear function u which is the dependent variable in a PDE (i.e., temperature, electric potential, pressure, etc.) The function can be approximated by a function using linear combinations of basis functions according to the following expressions (Nikishkov, 2004):

$$u \approx u_h \tag{3.36}$$

$$u = \sum_{n=1} u_i \psi_i \tag{3.37}$$

Where the u_i is the basic function assigned for each element, ψ_i is the coefficient of linear contribution of u_i to u_h. This function could be used to describe the 1D problem, for instance, the temperature dependence of the rod to its length (x) with non-uniformly heated.

The common points between 2 or more elements are called nodes. The values of the studied property computed at the nodes are used to approximate the values at non-node points (that is, in the element interior). For each element, the relation between the node's value and the coordinate variation is described by an Interpolation function or shape function. For the three-node triangle example, the value of an interior point could be approximated as:

$$\varphi(x,y) = N_1(x,y)\varphi_1 + N_2(x,y)\varphi_2 + N_3(x,y)\varphi_3 \tag{3.38}$$

Where $N1, N2, N3$ are the interpolation functions and $\varphi_1, \varphi_2, \varphi_3$ are the nodes' value.

3.2.4 Algorithms

The FEM calculation can be briefly described (Nikishkov, 2004) as follow:

- Discretize the continuum.
- Select interpolation functions.
- Find the element properties.
- Assemble the element equations.
- Solve the global equation system.
- Compute additional results.

3.3 Model definition

In this section, the two finite element models were describes in succession. A summary of differences between the two models were presented in the Table 3.1.

Table 3.1: Comparison of the two finite element models.

	Finite element model 1	Finite element model 2
Modelling object	A fermentation batch consists of a medium solution and a whole perimeter of the yeast-contained material.	A small part of the material with only a few yeast resides in.
Scale of the object	In millimeter	In micrometer
Simulated processes	Fermentation, Mass transportation	Fermentation, Mass transportation, and Mechanical properties
Model	Axial symmetric 2D	3D
Mesh style	2D free-triangular (A)	Free-tetrahedral (A)
Solver	MUMPS, Fully-coupled approach (A)	GMRES and Geometric multigrid solvers, Segregated approach (A)

3.3.1 Finite element model 1

A finite element modelling is described in detail in this section in which the fermentation process is coupled with mass transportation. Figure 3.5 shows how the fermentation batch was setup in the experiment. The batch contains a perimeter of a yeast-contained material and 5 ml of medium solution.

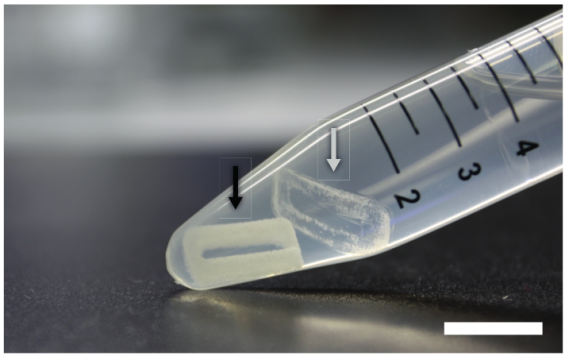

Figure 3.5: Fermentation batch with the material in the experiment (Priks et al., 2020).

a. Geometry

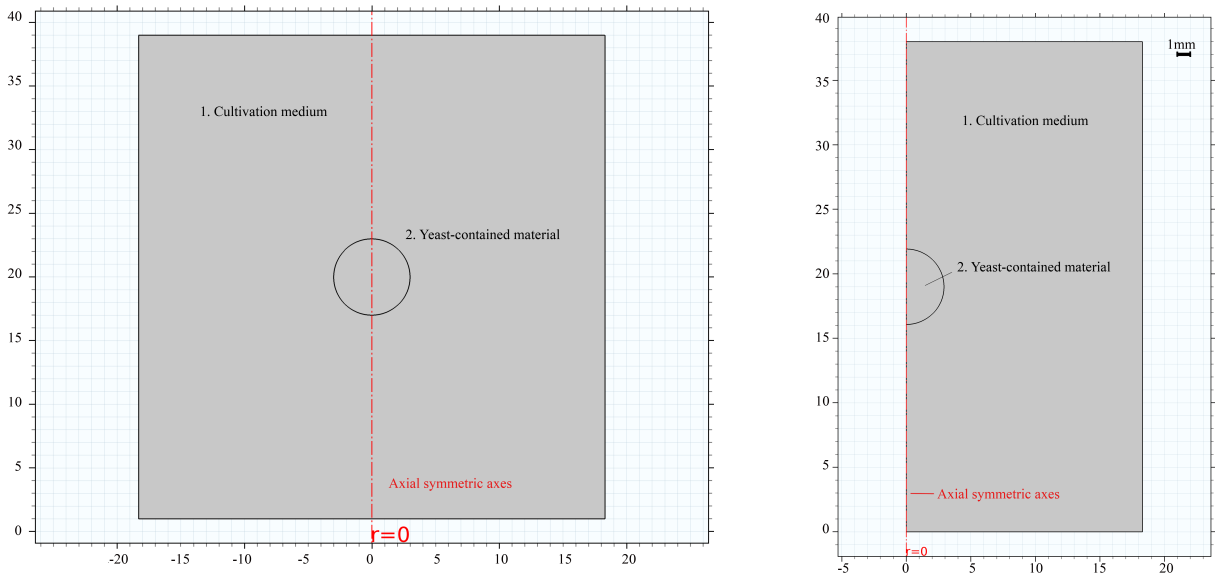

(a) Vertical cross-section of the cylindrical reactor batch

(b) Half-symmetric geometry of (a).

Figure 3.6: Geometry of the finite element model 1

.

For simplification, the model was built with two assumptions. First, the batch is a cylinder with a volume of 5 ml. Second, the material piece is assumed to have a sphere shape and all yeast cells are captured in this sphere area with a uniform distribution.

The model was created in the COMSOL-Multiphysics 5.2 software to simulate the fermentation and transportation processes in the system. Figure 3.6 presents the geometry of the model which illustrates a half cross-session of a batch system with the yeast-contained material placed in the center.

b. Boundary conditions

There are three boundary conditions were applied to the model (Figure 3.7). First, the boundary condition A is the axial symmetry of the model. Second, the boundary condition B constrains the yeast inside the sphere area where other compounds are able to travel between the yeast sphere and outer medium. Third, the boundary condition C is an imposed border in which there is no flux happens.

c. Expectations from the model

The model is able to show these desired features:

- During the fermentation, the distribution of reactants and products are non-uniform due to the delays in mass transportation.

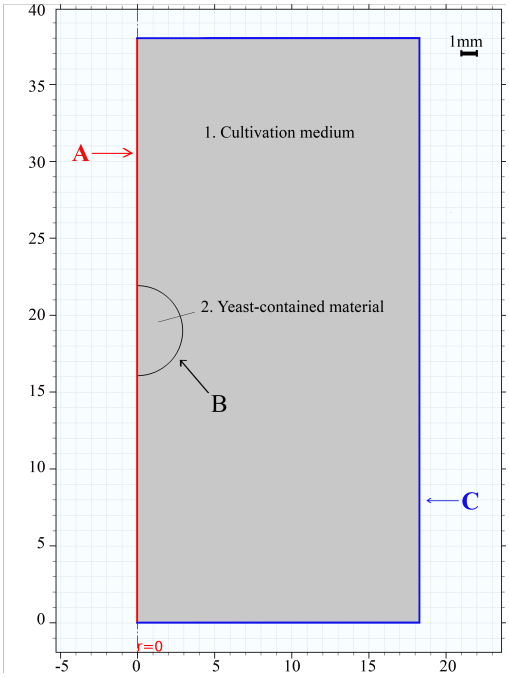

Figure 3.7: Boundary conditions of the model

- The growing of yeast in this model is slower compares to the one in the numerical model where the mixture is perfectly stirred.

3.3.2 Finite element model 2

A 3D finite element model is described in detail in this section. In this model, besides simulating the fermentation process and the mass transportation as in the finite element model 1, the solid mechanics were added to consider the mechanical properties of the material as well as its affects to the fermentation process.

a. Geometry

Figure 3.8 presents the micrographs of the yeast-contained material. Based on these pictures, a 3D symmetric model was created in the COMSOL-Multiphysics 5.2 software to study the mechanical properties of the material.

Figure 3.9 presents the geometry of the model which illustrates a small quarter-part of the printed material, in which:

- There are 4 spherical domains with a radius of 2.5 μm, each of them contains a single yeast cell.
- The cylinder presents the hydrogel matrix, its dimensions are 100 μm in height and 50 μm in the base radius.

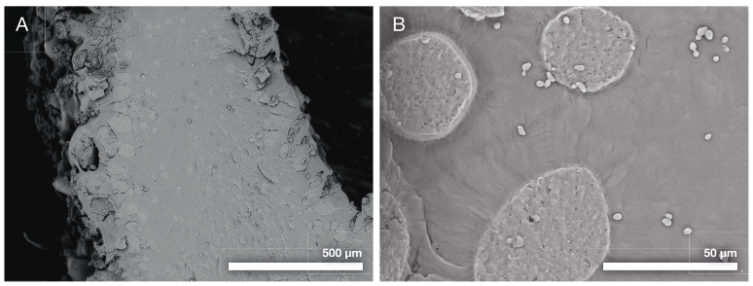

Figure 3.8: Micrographs of the yeast-contained material (Priks et al., 2020).

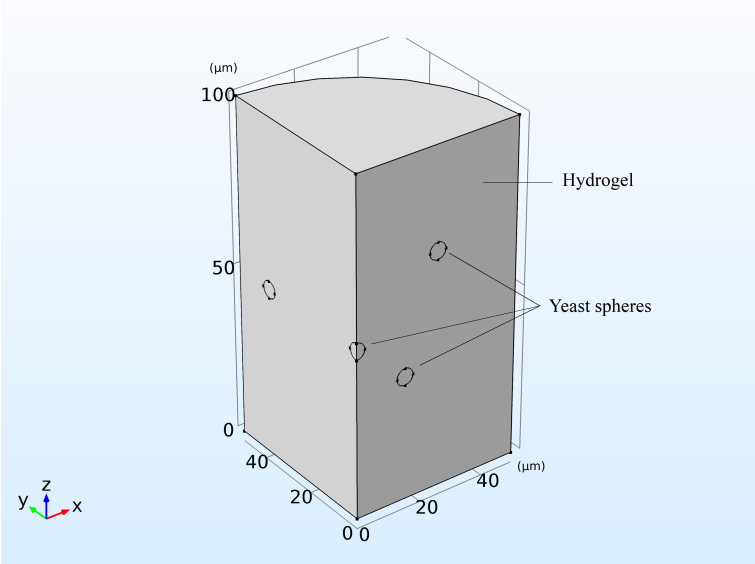

Figure 3.9: Geometry of the 3D finite element model

b. Boundary conditions

There are three boundary conditions were applied to the model (Figure 3.10) as follow:

- Symmetry conditions including the symmetry surfaces, symmetry axis, and the prescribed displacement point.
- Surface boundary 1:

– These are the surface boundaries in which glucose and fermentation products are allowed to penetrate through. Besides, glucose is continuously supplied through these surfaces to the inner yeasts from the outer environment.

– No displacement restrictions apply to these surfaces when calculating the mechanical properties.

- Surface boundary 2:

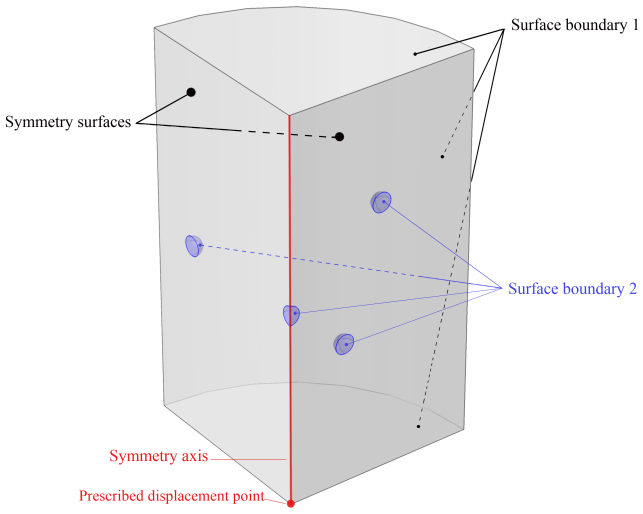

Figure 3.10: Boundary conditions of the model

– These boundary surfaces constrain the yeast inside the sphere area with the condition that each sphere is occupied by a single yeast cell. Other molecules are allowed to travel between the material matrix and the yeast cell through these surface.

– These surfaces are also the borders between two different material - the hydrogel and yeasts - which have different elastic properties; therefore leading to different stress and strain contours around these boundary surfaces.

c. Expectations from the model

The model is able to show these desired features:

- During the fermentation, the growth of yeast causes stress to the hydrogel matrix.
- When the stress on the material reaches a maximal possible value in which yeasts are able to replicate, the yeast growing process is stopped while glucose fermentation still happens.
- Yeast in each sphere has a different growing rate, i.e. has a different number of yeast cells at the end of the simulation, since it has different locations which effects to mass transportation and mechanical properties.

Chapter 4

Results and Discussion

4.1 Numerical models

This section presents results and discussion for the numerical models which were described at section 3.1.1. The two fermentation models - model 1 (section 3.1.1.b.) and model 2 (section 3.1.1.c.) were computed with optimizations to adapt to the experimental data.

4.1.1 Fermentation model 1

a. Validation

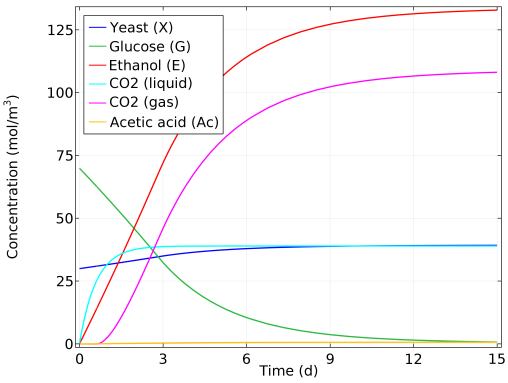

Figure 4.1: 1st simulation of the beer model

The results are shown at Figure 4.1. This model worked corresponding to the results of the brewing beer model at (Ramirez and Maciejowski, 2012). During the first 5 days, the number of yeasts grew rapidly resulting in significant production of ethanol and carbon dioxide while the concentration of glucose was declined. Coming to the 2nd period, 5th day to 10th day, since the remained glucose concentration was limited and the reaction rate depends on the glucose concentration (Eq. 3.1,3.2), either the producing rate of products or growth rate of yeast were decreased,

leading to curves' flatten. The last 5 days of the simulation shows steady states of all compounds due to the shortage of glucose.

b. Simulation

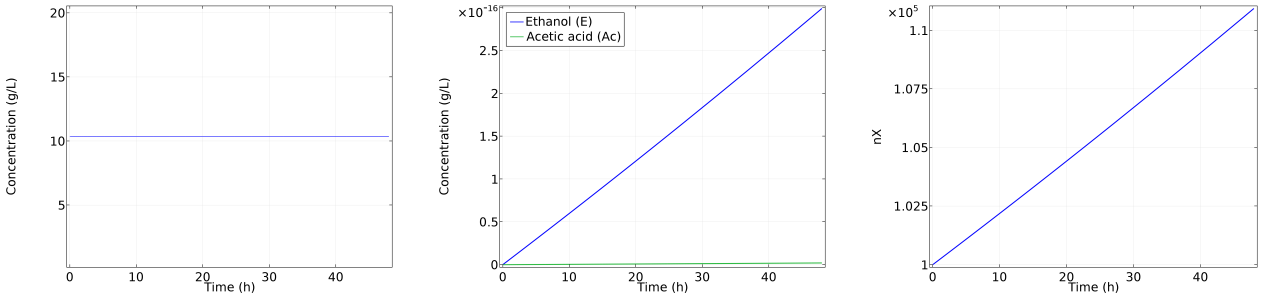

(a) Glucose concentration (b) products' concentrations (g/L) (c) Number of yeast cells

Figure 4.2: Simulation of the beer model with 10^5 yeast cells as the initial number of yeast

Figure 4.2 showed the model's output in which the concentration of glucose changes insignificantly and remained almost constant after 48 hours. In order to validate the model, its outputs were compared with the experimental data of the products' concentration and the number of yeast cells in the Table 2.4. Regarding the products' concentration, the produced ethanol and acetic acid were much smaller comparing to the experimental data. The number of cells after 40 hours was also much more modest comparing to the data in Table A.1 - $1,1.10^5$ cells vs. 4.10^8 cells, respectively.

Another simulation was carried out in which the growth rate of yeast was adjusted so that the number of yeast cells after 48 hours of cultivation is matched with the experimental data. For that, a correcting number was used incorporated with Y_X - yeast yield coefficient so that the new Y_X was 75 times larger than the value of Y_X in the previous model. Other parameters and initial conditions remained the same. The results were presented in the Fig.4.3.

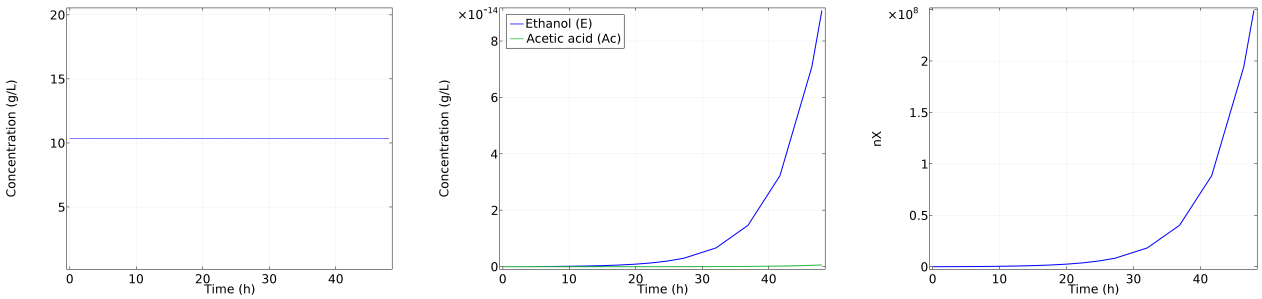

(a) Glucose concentration (b) products' concentrations (g/L) (c) Number of yeast cells

Figure 4.3: Simulation of the beer model with the adjusted Y_X

Since a correcting number was used for the yeast growth rate, the simulation gave a reasonable outcome for the number of yeast after 48h of the fermentation process, which was matched to the experimental data. However, the consuming glucose rate and production of ethanol, acetic acid reflected a big gap with data in Table A.1, leading to a question about the reliability of this model in this case.

In conclusion, this fermentation model had a low sensitivity which did not work accurately in the small system with a low concentration of spices. However, it initiated a good picture of fermentation processes and its reaction kinetics, leading to further advanced simulations.

4.1.2 Fermentation model 2

a. Validation

Figure 4.4 presented the results of this calculation which were corresponding to the ones in the referred model (Ariyajaroenwong et al., 2016). During the first 20 hours, the yeast and ethanol concentrations grew rapidly while the glucose concentration dropped. From 20th-hour to 30th-hour of the simulation, since the remained glucose concentration in the batch was low, the growth of yeast happened slowly. The 30th-hour to 40th-hour period showed a steady-state of yeast when the ethanol concentration reached 83.35 g/L (the maximal possible ethanol concentration in which yeast is able to grow); however, the ethanol production still occurred. The glucose fermentation process stopped, while the ethanol concentration got close to the maximal possible ethanol concentration in which the fermentation process might happen - 107.79 g/L, during the last 20 hours of the simulation.

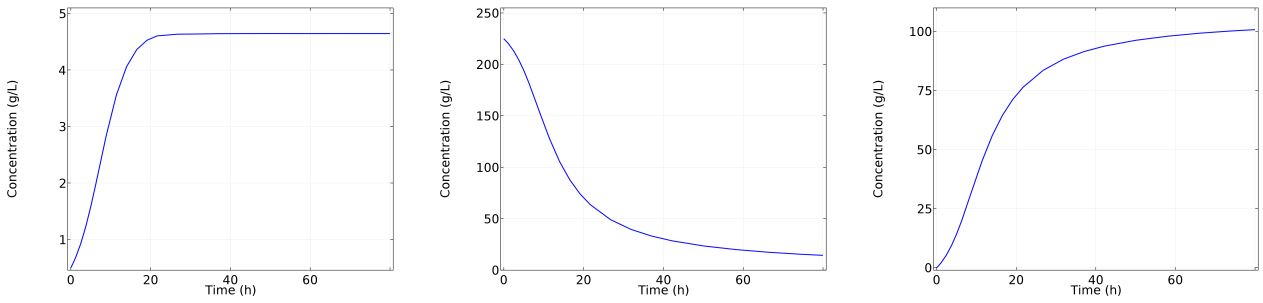

(a) Yeast concentration (b) glucose concentrations (g/L) (c) Ethanol concentration

Figure 4.4: Simulation of the sweet sorghum stalk model.

b. Simulation

Table 4.1 presents the computed data from the model in comparison with the experimental data. Regarding concentration of glucose, the computed concentration was slightly smaller compares

Table 4.1: Comparison of outcomes from the model to experimental data.

	Glucose (g/L)	Ethanol (g/L)	Δm_{wet} (mg)	n_{cell} final
Initial concentration	10.347	0	0	10^5
After 48h in the experiment	7.25	1.40	52.01	$3,93.10^8$
After 48h in the simulation	7.21	1.49	55.24	$3,97.10^8$

to the experimentally one (0.55%). In contrast, the concentration of ethanol in the model was 6.4% larger than in the experiment. Either amount of yeast or mass increment of yeast, which was characterized by Δm_{wet}, in the simulation were moderately differ from the data from the experiment ones.

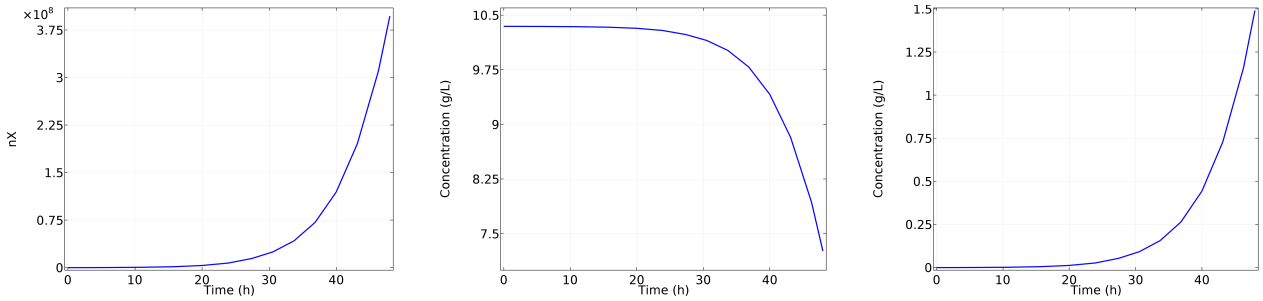

(a) Number of yeast cells (b) Glucose concentrations (c) Ethanol concentrations

Figure 4.5: Concentration of compounds over time in the model.

Nevertheless, the errors between experimental data and computational data were not significant and could be acceptable. This model also showed all the essential nature of the fermentation process. Thus, this model would be used as the fermentation model for the later simulations.

4.2 Finite element model 1

This section presented results and discussion for the finite element model 1 which was described at the section 3.3.1. During this section, mass transportation and its effect on the fermentation were considered.

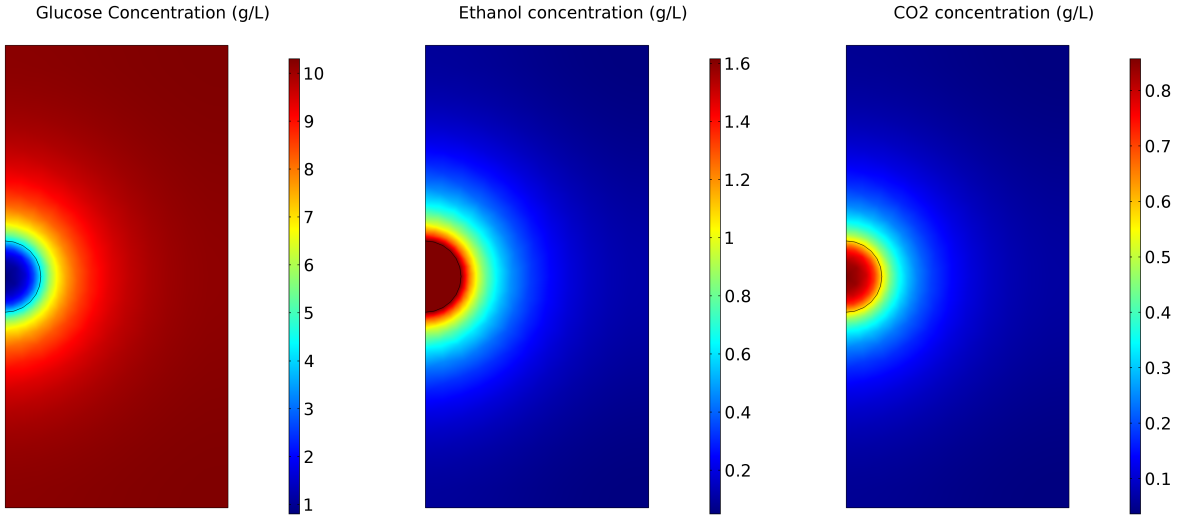

(a) Glucose (b) Ethanol (c) CO2

Figure 4.6: Concentration of reactant and products after 48h (g/L)

Figure 4.6 demonstrated the concentration distribution of different compounds in the 2D model after 48 hours of the fermentation simulation. Since different materials have different mass transportation properties, there is a significant difference in compounds' distribution between yeast domain and its surrounding environment.

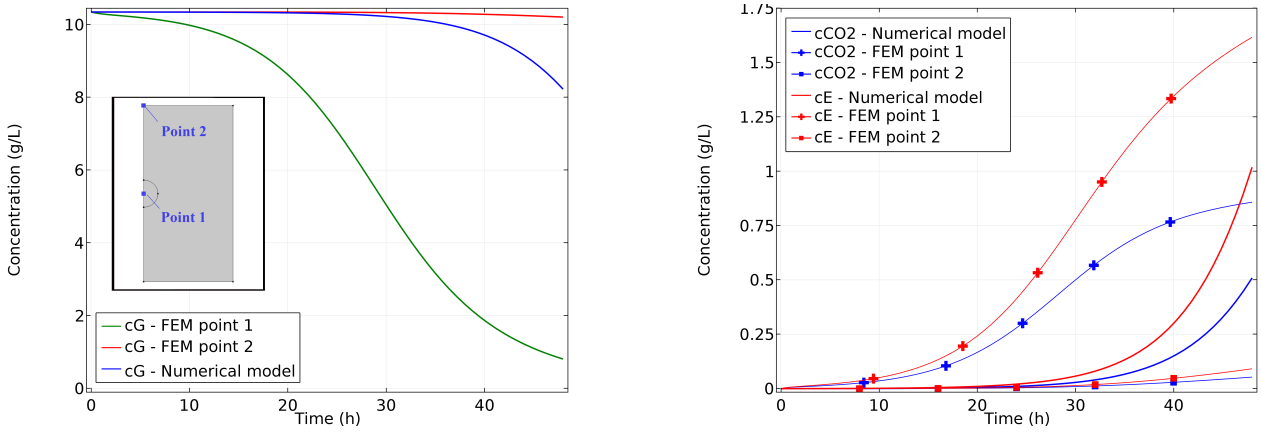

(a) Glucose (b) Fermentation products

Figure 4.7: Comparison of compounds' concentrations in different locations vs. the numerical model

In addition, the compounds' concentrations at different locations in geometry were presented in Figure 4.7, with concentration lines from the numerical model as a reference.

In Figure 4.7a, the glucose concentration at point 1, which located at the center of the yeast sphere, dropped dramatically faster comparing to the one at point 2. Since the glucose fermentation occurred only at the central sphere where the yeasts distributed, only glucose there was consumed in the reaction. The moving of glucose from the outer part i.e. point 2 to point 1 happened slowly due to the limitation in mass transportation. This was also the reason for the fact that the glucose in the numerical model was consumed slower than the one at point 1, but faster than the one at point 2 since in the numerical model, the reactor batch was assumed to be perfectly stirred and there was no transportation limitation.

By the same philosophy, the fermentation products' concentrations in the numerical model increased faster than the one at point 2 in the FEM model but slower than the one at point 1 in the FEM model, which were presented in the Figure 4.7b.

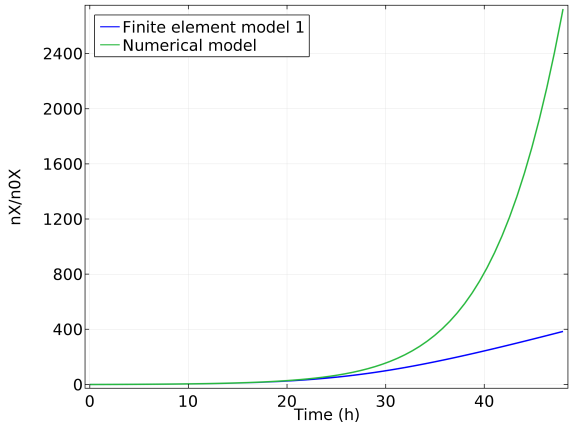

Figure 4.8: Comparison of the normalized number of yeast cells

Figure 4.8 shows the comparison of the normalized number of yeasts between the results from this calculation to the ones in the numerical model at the section 4.1.2.b.. The limited transportation of molecules, in fact, slowed down the yeast growing process, approximately 8 times slower comparing to the one in the numerical model.

4.3 Finite element model 2

This section presents results and discussion for the finite element model 2 which was described in section 3.3.2. In this model, the mechanical properties of the material and its effect on the fermentation are discussed in addition to the transportation limitation factor. A part of the results was published in (Nguyen et al., 2019).

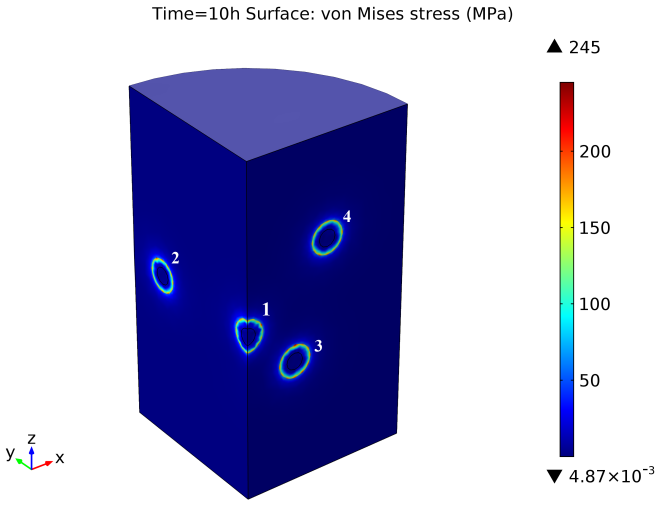

Figure 4.9: The expansion of yeast spheres and its effect to the material

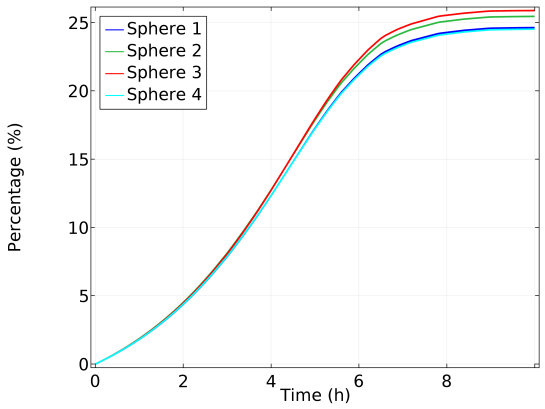

(a) Radius's increment of yeast spheres during the simulation.

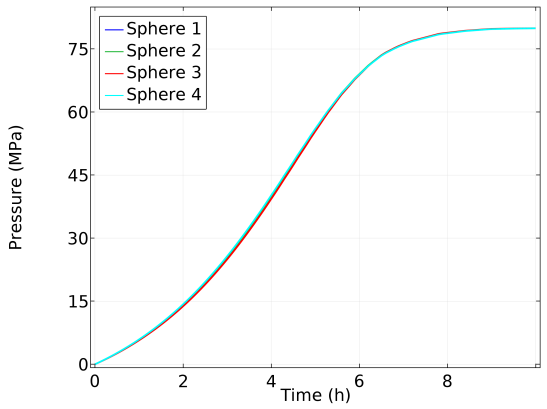

(b) Average pressure on the boundaries around yeast spheres.

Figure 4.10: The growing of yeast in different spheres limited by a pressure factor

.

During the fermentation process, the number of yeast cells increased, leading to an expansion in the volume of each sphere. Since the yeast spheres located in a solid material background, its volume expansion caused stress to the material, especially the areas surrounding the yeast domains. Figure 4.10a showed a normalized graph of spheres' radii in ten hours of simulation. These radii increased by approximately 25% comparing to the initial ones. This increase caused stress to the material with the average amplitude about 100-150 MPa, is illustrated in Figure 4.9.

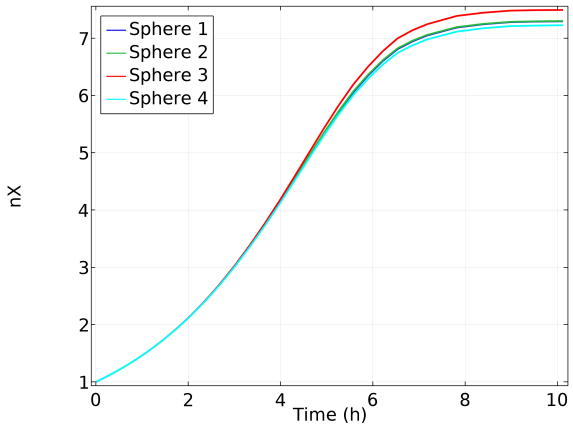

(a) Average numbers of yeast

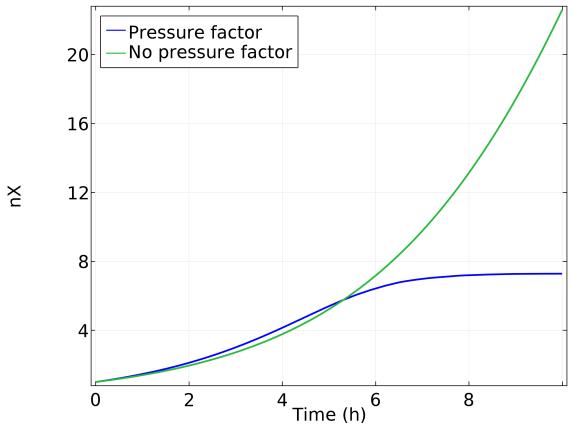

(b) Comparison of the yeast growth between the model with and without a limited pressure factor.

Figure 4.11: Number of yeasts and its comparison.

On the other hand, the produced stress introduced a feedback loop that inhibits the yeast growing process. When the stress reaches a certain value, the yeast stops to grow. This phenomenon was illustrated through Figure 4.10b and 4.11a in which the number of yeast approached a steady-state (around 7.3 cells in average per sphere) when the average pressure is approximately 70 MPa. This pressure condition is matching with other research in (Fernandes, 2005).

Besides, when comparing to the yeast growth in this model with the result in the case the limited pressure factor was not presented (Figure 4.11b), the number of yeast in this model is four times smaller. Thus, the pressure limitation is profoundly essential in the future developing model, contributing to an ideal model that simulates more precisely the whole material system.

Chapter 5

Summary

This study introduced a computational model that simulates all essential chemical and physical processes of the yeast-contained material when it involved in the glucose fermentation. The model helps people to understand the material properties, including the bio-catalytic activity in the fermentation, the mass transportation, and mechanical properties of the material and how they affect to the material catalysis.

The model can work as a quantitative prototype to study the catalysis property of the material in glucose fermentation. However, further experimental data are needed, especially data from experiments with different initial conditions such as temperature, pressure, pH value of the cultivation medium, to obtain a more precise model which can be used to pre-estimate cultivation time and amount of fermented products for a target system while knowing initial setup, and vice versa.

Regarding mass transportation and mechanical processes, this study illustrated satisfactorily the nature of these processes in the material during the fermentation. For future works, using additional experimental data that characterizes the diffusion in this material type and the elastic properties of the material, the model can be extended for such quantitative calculations. Additionally, further advanced mesh methods and optimizations in the geometry solver need to be implemented to achieve better results for the calculations regarding elastic processes in the material.

Acknowledgments

I would like to express appreciation to my supervisor Vahur Zadin for his extraordinary supports in this research.

Besdies, I would like to thank Hans Priks, Tobias Butelmann, and other people in the Intelligent Materials and Systems Laboratory and the ERA Chair in Synthetic Biology for providing me with data and information from experiments.

I take this opportunity to express gratitude to all of the Department faculty members and my friends for their help during the time I studied at the University of Tartu. I also thank my parents for the unceasing encouragement and support to make this studying abroad possible.

Bibliography

Aiba, S., Shoda, M., and Nagatani, M. (1968). Kinetics of product inhibition in alcohol fermentation. *Biotechnology and Bioengineering*, X:845,864.

Amestoy, P., Duff, I., and L'Excellent, J.-Y. (2000). Multifrontal parallel distributed symmetric and unsymmetric solvers. *Computer Methods in Applied Mechanics and Engineering*, 184(2):501 – 520.

Andrews, J. F. (1968). A mathematical model for the continuous culture of microorganisms utilizing inhibitory substrates. *Biotechnology and Bioengineering*, 10(6):707–723.

Ariyajaroenwong, P., Laopaiboon, P., Salakkam, A., Srinophakun, P., and Laopaiboon, L. (2016). Kinetic models for batch and continuous ethanol fermentation from sweet sorghum juice by yeast immobilized on sweet sorghum stalks. *Journal of the Taiwan Institute of Chemical Engineers*, 66:210–216.

Astrakhantsev, G. (1971). An iterative method of solving elliptic net problems. *USSR Computational Mathematics and Mathematical Physics*, 11(2):171 – 182.

B, P. and A., G. (2008). Yeast cell factories for fine chemical and api production. *Microb Cell Fact.*, 7:25.

Beidokhti], H. N., Janssen, D., Khoshgoftar, M., Sprengers, A., Perdahcioglu, E. S., den Boogaard], T. V., and Verdonschot, N. (2016). A comparison between dynamic implicit and explicit finite element simulations of the native knee joint. *Medical Engineering & Physics*, 38(10):1123 – 1130.

Bleve, G., Lezzi, C., Chiriatti, M., D'Ostuni, I., Tristezza, M., Venere, D. D., Sergio, L., Mita, G., and Grieco, F. (2011). Selection of non-conventional yeasts and their use in immobilized form for the bioremediation of olive oil mill wastewaters. *Bioresource Technology*, 102(2):982 – 989.

COMSOL, Inc. (2015). Fermentation in beer brewing. In: Comsol Multiphysics Documentation, Version 5.2.

D, E., F, G., and C, S. (1992). Determination of glucose and ethanol effective diffusion coefficients in ca-alginate gel. *Enzyme Microb Technol.*, 14:396–401.

Entwistle, K. M. (2001). *Basic Principles of the Finite Element Method.* Maney.

Fernandes, P. (2005). How does yeast respond to pressure? *Brazilian Journal of Medical and Biological Research*, 38:1239 – 1245.

Fick, A. (1995). On liquid diffusion. *Journal of Membrane Science*, 100(1):33–38.

GP, C. and JM., C. (1999). Applications of yeast in biotechnology: protein production and genetic analysis. *Curr Opin Biotechnol.*, 10:422–7.

Haynes, W. M. (2012). *Handbook of Chemistry and Physics*. CRC Press.

Hiester, H., Piggott, M., Farrell, P., and Allison, P. (2014). Assessment of spurious mixing in adaptive mesh simulations of the two-dimensional lock-exchange. *Ocean Modelling*, 73:30–44.

Ito, K., Inthavong, K., Kurabuchi, T., Ueda, T., Endo, T., Omori, T., Ono, H., Kato, S., Sakai, K., Suwa, Y., Matsumoto, H., Yoshino, H., Zhang, W., and Tu, J. (2015). Cfd benchmark tests for indoor environmental problems: Part 1 isothermal/non-isothermal flow in 2d and 3d room model. *International Journal of Architectural Engineering Technology*, 2:01–22.

Laidler, K. J. (1987). *Chemical Kinetics 3rd E.* Harper & Row.

Levenspiel, O. (1980). The monod equation: A revisit and a generalization to product inhibition situations. *Biotechnology and Bioengineering*, 22(8):1671–1687.

Li, J. and Mooney, D. J. (2016). Designing hydrogels for controlled drug delivery. *Nature Reviews Materials*, 1(12).

Li, Z., Xiao, M., Lu, L., and Li, Y. (2008). Production of non-monosaccharide and high-purity galactooligosaccharides by immobilized enzyme catalysis and fermentation with immobilized yeast cells. *Process Biochemistry*, 43(8):896 – 899.

Liu, X., Tang, T.-C., Tham, E., Yuk, H.and Lin, S., and Lu, T. K.and Zhao, X. (2017). Stretchable living materials and devices with hydrogel-elastomer hybrids hosting programmed cells. *Proc. Natl. Acad. Sci. U. S. A.*, 114(9):2200–2205. PMID: 28202725.

Logan, D. L. (2011). *A first course in the finite element method*. SI Edition.

Malik, A. (2004). Metal bioremediation through growing cells. *Environment International*, 30(2):261 – 278.

Mathews, C., van Holde, K., and Ahern, K. (1999). *Biochemistry (3 ed.)*. Prentice Hall.

Murtey, M. and Ramasamy, P. (2016). *Sample Preparations for Scanning Electron Microscopy – Life Sciences*, pages 161–186.

Nguyen, P., Priks, H., Kumar, R., Lahtvee, P.-J., and Zadin, V. (2019). 3d - modeling of a yeast-containing hydrogel. *EuroHPC Summit Week - PRACEday19*.

Nikishkov, G. (2004). *Introduction to the Finite Element Method*. Lectures Notes. University of Aizu, Japan.

Onsager, L. (1945). Theories and problems of liquid diffusion. *Ann N Y Acad Sci.*

Piskur, J. and Compagno, C. (2004). *Molecular Mechanisms in Yeast Carbon Metabolism*. Springer.

PM, D. and JE., B. (1986). Effects of hydroxyurea on immobilized and suspended yeast fermentation rates and cell cycle operation. *Biotechnol Bioeng*, pages 01–22.

Priks, H., Butelmann, T., Illarionov, A., Johnston, T. G., Fellin, C., Tamm, T., Nelson, A., Kumar, R., and Lahtvee, P.-J. (2020). Physical confinement impacts cellular phenotype within living materials. *bioRxiv*.

Ramirez, D. A. G. W. F. (1994). A flavour model for beer fermentation. *Journal of The Institute of Brewing*, 100(5):321–329.

Ramirez, W. F. and Maciejowski, J. (2012). Optimal beer fermentation. *Journal of the Institute of Brewing*, 113(3):325–333.

Saad, Y. and Schultz, M. H. (1986). Gmres: A generalized minimal residual algorithm for solving nonsymmetric linear systems. *SIAM Journal on Scientific and Statistical Computing*, 7(3):856–869.

Saha, A., Johnston, T. G., Shafranek, R. T., Goodman, C. J., Zalatan, J. G., Storti, D. W., Ganter, M. A., and Nelson, A. (2018). Additive manufacturing of catalytically active living materials. *ACS Applied Materials & Interfaces*, 10(16):13373–13380. PMID: 29608267.

Solin, P. (2016). *Partial Differential Equations and the Finite Element Method.* John Wiley & amp; Sons.

SP, B., C, G., M, T., LR, P., TM, Y., and O., C. (2018). Mechanical feedback coordinates cell wall expansion and assembly in yeast mating morphogenesis. *PLoS Comput Biol.*, 14(1).

Willaert, R., Backer], L. D., and Baron, G. V. (1996). Modelling the immobilisation of cells in a packed bed of porous carriers. In Wijffels, R., Buitelaar, R., Bucke, C., and Tramper, J., editors, *Immobilized Cells*, volume 11 of *Progress in Biotechnology*, pages 154 – 161. Elsevier.

William D. Callister, J. t. e. (2007). *Material Science and Engineering - An Introduction*. John Wiley & Sons, Inc.

Zentou, H., Z., Z. A., YunusR., Biak, A., D. R., Z., and M., & Hassani, A. (2019). Modelling of molasses fermentation for bioethanol production: A comparative investigation of monod and andrews models accuracy assessment. *Biomolecules*, page 308.

Zhu, J. and Marchant, R. E. (2011). Design properties of hydrogel tissue-engineering scaffolds. *Expert Review of Medical Devices*, 8(5):607–626. PMID: 22026626.

Zhu, L., Qiu, J., and Sakai, E. (2017). A high modulus hydrogel obtained from hydrogen bond reconstruction and its application in vibration damper. *RSC Adv.*, 7:43755–43763.

Appendix A

Experimental data for fermentation process

Table A.1: Concentrations of compounds after 48h of cultivation. A = air supply, M = no air supply; dissolved oxygen did not drop below 30% (Priks et al., 2020)

ID	Glucose (g/L)	Acetic acid (g/L)	Glycerol (g/L)	Δm_{wet} (mg)	n_{cell} final
A2.1	7.92	0.03	0.22	55.26	$3,95.10^8$
A2.2	7.25	0.04	0.26	52.01	$3,93.10^8$
M1.5	7.46	0.04	0.28	52.01	$3,93.10^8$
M1.7	7.28	0.04	0.28	60.29	$4,31.10^8$

From the experimental data, the number of yeast cells after n-th day is calculated as:

$$n_{cell} = n^0_{cell} + \frac{\Delta m_{wet} * \%m}{m_{DW}} \tag{A.1}$$

Where n_{cell} and n^0_{cell} are the number of yeast at 0th day and after n-th day respectively, m_{DW} is the dry-weight mass of a single yeast cell ($2,8.10^{-11}$ gDW/cell (Willaert et al., 1996)), $\%m$ is the mass percentage between the dry weight and wet weight of a cell.

Besides, due to the lack of the ethanol concentration after 48 hours from the experiment, the ethanol concentration is estimated based on the ethanol - glycerol concentration ratio from the experimental data after the 7th day. Particularly, the ethanol concentration is 6.37 times larger than the glycerol concentration. Thus, the ethanol concentration in the system after 48h of cultivation is about 1.4 g/L.

Descriptions of the Finite element model 1

Material

Both domains (1 and 2) are surrounded by an aqueous medium which dissolves the glucose - the main nutrient source for yeast - and the fermentation products later. Besides, domain 2 is a yeast-contained hydrogel material in which the diffusion processes is more limited compared to the one in the aqueous medium (Table A.3).

Mesh

The model meshed with 2D free-triangular elements which have the maximum element size is 2,01 mm and the minimum element size is 0,0114 mm. The complete mesh consists of 634 domain elements and 74 boundary elements. The global mesh is presented in Figure A.1.

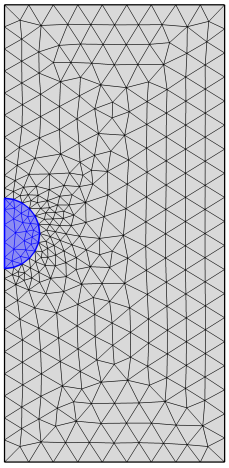

Figure A.1: The 2D mesh of the finite element model 1

Solver Configurations

The modelling system was computed by a MUltifrontal Massively Parallel sparse direct Solver (MUMPS) which is an application for solving large sparse systems of linear algebraic equations based on the Gaussian elimination (Amestoy et al., 2000). In this solver, a Fully coupled approach was chosen which solved all equations of known and unknowns components at once, in a single iteration. In a 2D model, this approach is more robust and time-efficient. Direct algorithms were used in this approach since the model was relatively simple so that these algorithms worked with reasonable time and compute resources.

Descriptions of the Finite element model 2

Material

All domains are surrounded by an aqueous medium which dissolves the glucose - the main nutrient source for yeast - and the fermentation products later. The cylinder domain is the hydrogel material with its own properties while the spherical domains are yeast cells.

Mesh

The model meshed with free-tetrahedral elements which have the maximum element size is 8 μm and the minimum element size is 1 μm. The complete mesh consists of 11947 domain elements and 2000 boundary elements, and 188 edge elements. The global mesh is presented in Figure A.2.

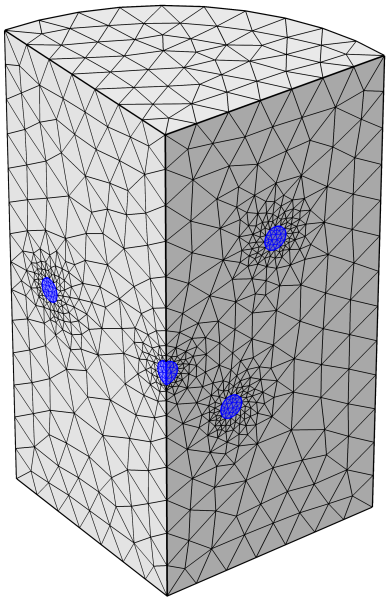

Figure A.2: The 3D mesh of the 3D finite element model 2

Solver configurations

In the solver of this model, a Segregated approach was chosen which subdivides the problem into segregated steps rather than solves all equations at once. Each segregated step is either an equation system of a single physics or multi-physics, but usually smaller than the full system of equations that are formed with the Fully Coupled approach. These steps are solved serially in each iteration, thus requires more calculation time while less computing resources.

The equation system was solved by with the Generalized minimal residual method (GMRES) solver - an iterative solver that is often used to solve nonsymmetric system of linear equations (Saad

and Schultz, 1986).

In addition, a geometric multigrid solver was also used to accelerates the convergence of the iterative solver. This solver solves series of meshes rather than a single one as a result of auto-build adaptive meshes with courser sizes compares to the initial mesh size (Astrakhantsev, 1971).

Boundary condition equations

There are three boundary conditions were applied to the model (Figure 3.10) as follow:

- Symmetry conditions at:

– The symmetric surfaces:

$$n.u = 0$$

– The symmetric axes:

$$u = u_{0x}; v = u_{Oy}$$

- The prescribed displacement point:

$$u = 0$$

- Surface boundary 1:

– These are the surface boundaries in which glucose and fermentation products are allowed to penetrate through. Besides, glucose is continuously supplied through these surfaces to the inner yeasts from the outer environment.

$$c_i = c_{0,j}$$

– No displacement restrictions apply to these surfaces when calculating the mechanical properties.

- Surface boundary 2:

– These boundary surfaces constrain the yeast inside the sphere area with the condition that each sphere is occupied by a single yeast cell. Other molecules are allowed to travel between the material matrix and the yeast cell through these surface.

$$-n.N_j = 0$$

– These surfaces are also the borders between two different material - the hydrogel and yeasts - which have different elastic properties; therefore leading to different stress and strain contours around these boundary surfaces.

$$\varepsilon = \beta_v.\Delta n_{cells}$$

Kinetics parameters for chemical reactions

Table A.2: Coefficients for fermentation models.

Notation	Value	Unit	Explaination
A_G	$9,51.10^{11}$	$1/s$	The frequency factor of the fermentation reaction
E_a	$9,46.10^4$	J/mol	The activation energy of the fermentation reaction
T	20	$^\circ C$	Temperature
A_{IG}	$2,0897.10^{-53}$	mol/m^3	The frequency factor of glucose inhibition
E_I	$-2.8702.10^5$	J/mol	The activation energy of glucose inhibition
K_x	365000	mol^2/m^6	The yeast growth inhibition constant
K_{GL}	0.07	h^{-1}	Gas to liquid transfer coefficient
$c_{CO2(sat)}$	39	mol/m^3	The saturated carbon dioxide concentration in water
Y_x	0.134	/	Yield coefficient of yeast
Y_E	1.92	/	Yield coefficient of ethanol
Y_{CO2}	1.97	/	Yield coefficient of carbon dioxide
Y_{Ac}	0.01	/	Yield coefficient of acetic acid
Y_G	1	/	The consuming coefficient of glucose
$\mu_{X_{max}}$	0. 313	h^{-1}	The maximum specific growth rate of yeast
K_G	47.51	g/L	The half-velocity constant
$I_{G/X}$	308.13	g/L	The glucose inhibition constant for yeast growing
$c_{E_{max}/X}$	83.35	g/L	The maximum ethanol concentration for yeast growing
$\mu_{E_{max}}$	3.69	h^{-1}	The maximum specific producing rate of ethanol
K_E	28.39	g/L	The ethanol saturation constant
$I_{G/E}$	299.67	g/L	The glucose inhibition constant for ethanol production
$c_{E_{max}/E}$	107.79	g/L	The maximum ethanol concentration for ethanol production
$Y_{X/G}$	0.5	g/g	The yeast yield coefficient
$Y_{E/G}$	0.48	g/g	The ethanol yield coefficient
m	0.001	h^{-1}	The cell maintenance coefficient
α, β	1.53	g/L	The ethanol inhibition constant
P_{max}	10^8	Pa	The critical pressure of yeast

Diffusion coefficients

Table A.3: Diffusion coefficient of compounds in the model. [1] are from (Haynes, 2012), [2] are from (D et al., 1992), [3] is an estimated value.

Compound	Value ($\mu m^2/s$)	Environment
Glucose	600[1]	Water
Ethanol	1076[1]	Water
Carbon dioxide	1600[1]	Water
Glucose	510[2]	Hydrogel
Ethanol	960[2]	Hydrogel
Carbon dioxide	1200[3]	Hydrogel

Non-exclusive licence to reproduce thesis

I, Thi Bich Phuong Nguyen,

1. Here with grant the University of Tartu a free permit (non-exclusive licence) to reproduce, for the purpose of preservation, including for the purpose of preservation in the DSpace digital archives until the expiry of the term of copyright,

Modelling of a Yeast-contained Material

supervised by Ph.D. Vahur Zadin.

Publication of the thesis is not allowed.

2. I am aware of the fact that the author retains the right specified in p. 1.

3. This is to certify that granting the non-exclusive licence does not infringe other persons' intellectual property rights or rights arising from the personal data protection legislation.

Thi Bich Phuong Nguyen, **20.05.2020**